Grid Cell Hexagonal Patterns Formed by Fast Self-Organized Learning Within Entorhinal Cortex

Himanshu Mhatre,[1,2] Anatoli Gorchetchnikov,[1,2] and Stephen Grossberg[1,2*]

ABSTRACT: Grid cells in the dorsal segment of the medial entorhinal cortex (dMEC) show remarkable hexagonal activity patterns, at multiple spatial scales, during spatial navigation. It has previously been shown how a self-organizing map can convert firing patterns across entorhinal grid cells into hippocampal place cells that are capable of representing much larger spatial scales. Can grid cell firing fields also arise during navigation through learning within a self-organizing map? This article describes a simple and general mathematical property of the trigonometry of spatial navigation which favors hexagonal patterns. The article also develops a neural model that can learn to exploit this trigonometric relationship. This GRIDSmap self-organizing map model converts path integration signals into hexagonal grid cell patterns of multiple scales. GRIDSmap creates only grid cell firing patterns with the observed hexagonal structure, predicts how these hexagonal patterns can be learned from experience, and can process biologically plausible neural input and output signals during navigation. These results support an emerging unified computational framework based on a hierarchy of self-organizing maps for explaining how entorhinal-hippocampal interactions support spatial navigation. © 2010 Wiley-Liss, Inc.

KEY WORDS: grid cells; entorhinal cortex; self-organized learning; path integration; spatial navigation

INTRODUCTION

A Hierarchy of Self-Organizing Maps

The discovery of grid cells in the entorhinal cortex (Hafting et al., 2005) has excited renewed interest in the field of animal navigation. Grid cells are found predominantly in superficial layers of the dorsal medial entorhinal cortex (dMEC) and get activated at locations corresponding to the vertices of a hexagonal lattice that spreads uniformly across the environment (Hafting et al., 2005; Sargolini et al., 2006). The lattice structure of neighboring cells has a similar period but is spatially offset in phase. Furthermore, the spacing of this lattice changes for the cells along the dorsomedial-ventrolateral gradient in the entorhinal cortex, with progressively larger spacing for more ventral cells (Hafting et al., 2005). Since the entorhinal cortex is the source of primary input to the hippocampus, it is thought that grid cells play a crucial role in the development of place cells (Rolls et al., 2006; Solstad et al., 2006).

Multiple models have proposed that a combination of grids of multiple spatial scales can lead to single-peaked place fields (Fuhs and Touretzky, 2006; McNaughton et al., 2006). Furthermore, Gorchetchnikov and Grossberg (2007) have demonstrated how an entorhinal-hippocampal self-organizing map can learn the relationships between grid cell fields of multiple spatial scales and to give rise to hippocampal place fields that are capable of representing much larger, and behaviorally useful, spatial scales for navigation; indeed, hippocampal place cells whose spatial scale is the lowest common multiple of spatial periods of the entorhinal grid cells that activate them. This result raises the question of whether a self-organizing map can also learn to generate the hexagonal shape of grid cell fields themselves, thereby providing a unified explanation of the emergence of entorhinal-hippocampal spatial representations based on a hierarchy of self-organizing maps that convert the linear velocity and angular velocity signals which result from an animal's navigational movements into progressively larger scales of spatial representation (Fig. 1).

The current model builds on a general observation about the trigonometry of spatial navigation in a two-dimensional environment. This observation explains in a simple way why hexagonal grid cell patterns may be favored when an animal navigates. It also clarifies why a self-organizing map mechanism can naturally learn to generate hexagonal grid cell firing patterns while an animal navigates in an open environment. These results were briefly reported in Mhatre et al. (2009a,b).

The authors of the interference model of grid cell formation have previously suggested that some process of self-organization could be responsible for the hexagonal shape of the grid structure (Burgess et al., 2007; Burgess, 2008). While their claim was not demonstrated by explicit model mechanisms or simulations, it emphasizes a growing consensus that self-organizing processes may play a key role in the formation of spatial representations in the brain. The interference model (Burgess et al., 2007) proposed that the hexagonal grid cell firing pattern may arise due to interference patterns that occur when three patterns of oscilla-

[1] **Department of Cognitive and Neural Systems, Center for Adaptive Systems, Boston University, Boston, Massachusetts;** [2] **Center of Excellence for Learning in Education, Science and Technology, Boston University, 677 Beacon St, Boston, Massachusetts**

Grant sponsor: CELEST, an NSF Science of Learning Center; Grant number: SBE-0354378; Grant sponsor: SyNAPSE Program (DARPA); Grant number: HR0011-09-C-0001.

*Correspondence to: Stephen Grossberg, Department of Cognitive and Neural Systems, Center for Adaptive Systems, Boston University, Boston, MA. E-mail: steve@bu.edu

Accepted for publication 9 September 2010
DOI 10.1002/hipo.20901
Published online in Wiley Online Library (wileyonlinelibrary.com).

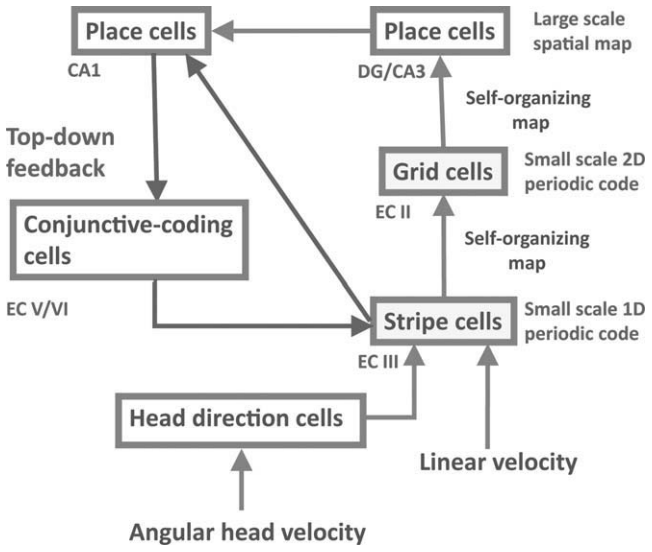

FIGURE 1. A system diagram of interactions within the entorhinal-hippocampal navigational system. The GRIDSmap model clarifies how stripe cells may give rise to grid cells via a self-organizing map. Earlier work of Gorchetchnikov and Grossberg (2007) demonstrated how grid cells may give rise to place cells via a self-organizing map. Together these results suggest that a hierarchy of self-organizing maps may learn key properties of the brain navigational circuits that are based on path integration signals. This figure also notes that other pathways (in red) exist in this navigational system, notably a direct pathway from entorhinal cortex to region CA1 in the hippocampus, and top-down feedback pathways from the hippocampal cortex to entorhinal cortex. The possible role of these top-down feedback pathways in stabilizing the learning in the self-organizing maps is noted in the Discussion section.

tion interact across space. Each spatial pattern of oscillation was assumed to have a linear band-like structure and the same spatial period. If three such oscillatory patterns have preferred directions that differ by 60°, then a hexagonal interference pattern will be generated if their product determines grid cell firing. In particular, Burgess et al. (2007, p 801) wrote: "These inputs cause the intrinsic oscillation of subunit membrane potential to increase above theta frequency by an amount proportional to the animal's speed of running in the "preferred" direction. The phase difference between this oscillation and a somatic input at θ-frequency essentially integrates velocity so that the interference of the two oscillations reflects distance traveled in the preferred direction."

This interference mechanism also implies that overlaying other sets of angular separations can generate markedly different grid cell firing patterns (Hasselmo et al., 2007). In particular, if the angular separations of the oscillations do not equal 60°, then their interference patterns can create a wide-range of nonhexagonal patterns. However, these other patterns are not observed in the firing fields of experimentally recorded cells. Thus a mechanism must exist that naturally selects the orientations that are 60° apart over all other possible orientation combinations.

The first contribution of the current article is the description of a simple trigonometrical relationship that exists between directional path integration inputs when an animal navigates in an open field. This relationship clarifies why hexagonal structures may arise from the most frequent co-occurrence patterns of these directional path integration inputs. The GRIDSmap neural model that is developed in this article shows how the most frequent co-occurrences can be detected, amplified, and learned by the interacting competitive, habituative, and associative mechanisms of a suitably defined self-organizing map, while less frequent cooccurrences are suppressed, even if there are more than three sources of path integration inputs, and even if they are not separated by 60°.

RESULTS

Model Description

The trigonometry of navigation: Why hexagonal patterns are favored

This insight about the trigonometry of spatial navigation is most easily understood in terms of path integration cells each of which fires periodically whenever an animal moves a fixed distance in the cell's favored direction. These cells are called stripe cells for reasons that will be made clear in the next section. The basic trigonometric insight holds independently of how such cells may be constructed, just so long as the cell firing patterns can be used to drive learning within a self-organizing map model such as GRIDSmap.

Let d_θ represent the distance traveled by the animal along the direction θ and let l be the period length of the stripe cells. Then the stripe cell oriented along direction θ will get activated whenever $d_\theta = nl$, with n equal to any integer 1, 2, 3,... Consider the coactivation of the stripe cell oriented at 0° with stripe cells oriented at other angles. The stripe cell oriented along 0° will also be activated whenever $d_0 = ml$, with m equal to any integer 1, 2, 3,... If the animal traverses distance d_0 along 0°, then its relative displacement along direction θ is:

$$d_\theta = d_0 \cdot \cos(\theta). \quad (1)$$

Coactivation of these two stripe cells will happen whenever both have covered multiples of lattice length; that is, when $d_\theta = nl$ and $d_0 = ml$. Substituting this constraint into Eq. (1) gives $nl = ml \cdot cos(\theta)$ or

$$\cos(\theta) = n/m \quad (2)$$

An example of this is shown in Figure 2 with $n = 4$ and $m = 5$. As the integers n and m increase, the distance needed to be traversed to reach the next location with coactivation also increases. The larger this distance, the less frequent the coactivations of these stripe cells will be while the animal runs in the environment. Thus, if we exclude the case of $n = m$, the most fre-

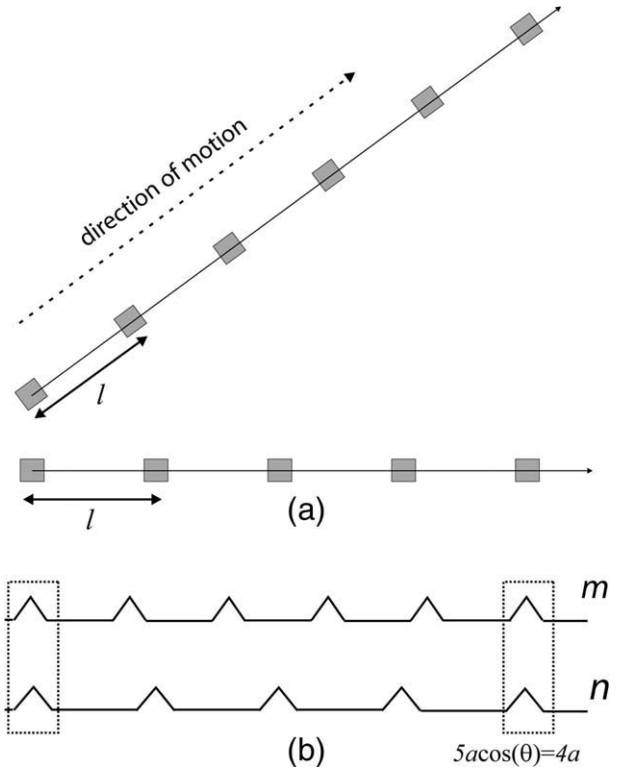

FIGURE 2. Mechanism of coactivation of stripe cells of different preferred directions. The animal is moving distance *l* along the direction marked with an arrow in panel (a). Two stripe cells with identical period *l* have directions as shown: one parallel to motion, another horizontal, with the angle θ between them. Gray squares show the areas of activity of both cells along their respective directions. Panel (b) shows the activity of these cells through time with dashed boxes highlighting the coactivation episodes. A perfect coactivations can only be achieved when *cos*(θ) is the rational number 4/5 in the shown example.

quent coactivations will occur for the smallest possible nontrivial values of n and m: $n = \pm 1$ and $m = \pm 2$, which leads to $\cos(\theta) = \pm[1/2]$, or $\theta = \pm 60^\circ \pm 180^\circ$. Note that due to the bidirectional nature of stripe cells, a 180° difference leads to the exact same angle, so it is sufficient to set $\theta = \pm 60^\circ$. Hence, most frequent coactivations will occur for angle differences between stripe cell orientations that are $\pm 60^\circ$ apart, and this can and will be emphasized by a suitably defined self-organizing map.

The model presented here verifies the simple reasoning above within a recurrent shunting on-center off-surround self-organizing map learning process (Grossberg, 1976a,b, 1978; contrast Kohonen, 1984) in the projections from stripe cells to the map cells that will learn to become grid cells. This mechanism is consistent with the hypothesis that stripe cells exist in Layer III or deeper layers of the dorsal segment of medial EC (dMEC) where conjunctive cells with some stripe-like properties have been recorded (Sargolini et al., 2006).

Stripe cells

Our neural model predicts that grid cells form their regular hexagonal pattern through a process of self-organized map learning based on input from stripe cells that code directional displacement. A similar construct formed by oscillatory interference and termed band cells was proposed in the initial presentation of the interference model by Burgess et al. (2005). The stripe cells proposed here are based on a different mechanism that is described below; hence the name stripe cell is used to avoid confusion.

Stripe cells are predicted to occur in Layer III of entorhinal cortex, where they input to the grid cells in Layer II. The displacement along a direction that is coded by a stripe cell is a measure of the relative distance covered by a navigating animal along that direction during a free movement in the environment. The linear velocity along a direction can be obtained by modulating a movement velocity signal with a head direction signal. Since the integration of velocity cannot continue indefinitely due to limited resources, at some point it has to reset back to zero and start again, in effect creating a periodicity in the output of the cells that are responsible for performing the integration operation.

A circuit that can generate the desired stripe cell periodicity and reset is a one-dimensional (1D) ring attractor whose cells are stripe cells with the same preferred direction and spatial period, but different positional selectivity. In such an attractor, an activity bump moves driven by input proportional to the projection of an animal's linear velocity on the preferred direction of the attractor circuit. When this projection is zero, the bump remains stationary so that the same cells remain active during this time interval. How are periodic output signals generated from a moving bump of activity in such a ring attractor? The ring has a finite length and closes upon itself, so the activity bump returns to the same position on the ring, and thus causes the same stripe cells to become active again, after a certain distance is traversed in the preferred direction. Stripe cells with different spatial phases become maximally active at different positions along such attractors. When observed in a freely moving animal, this periodicity will cause the firing of each cell in the ring to resemble parallel stripes oriented perpendicular to the cell's preferred direction; hence the name stripe cells.

Such periodicity in the context of linear velocity estimation limits the spatial scale of the path integration process. As a result, the stripe cells represent a 1D periodic spatial code of a scale of tens of centimeters (Fig. 1), which is much smaller than the scale of place cells capable of measuring distances at least as large as the sizes of the environments that animals typically navigate. To construct a two-dimensional (2D) large-scale place code from a 1D small-scale stripe cell code, a two step hierarchy of self-organizing maps is proposed. The first step in this hierarchy converts 1D stripe cells into a 2D periodic map of grid cells with multiple spatial scales. The second step, carried out in Gorchetchnikov and Grossberg (2007), converts grid cells of multiple spatial scales into a still larger-scale 2D map of place cells having a spatial scale equal to the least common multiple of the grid cell spatial scales.

The model presented here predicts that stripe cells collectively cover multiple directions and multiple spatial phases. A key feature of the model is the self-organization of these inte-

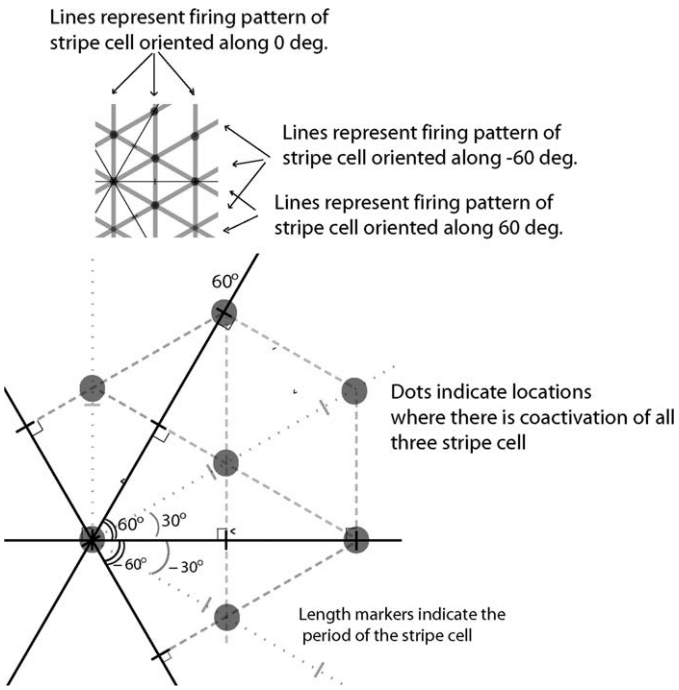

FIGURE 3. Trigonometric principles underlying hexagonal structure formation. Intersection of stripes oriented at multiples of 60° forms a hexagonal structure (top plot). This coactivation is based on relative velocity integration (bottom plot) as demonstrated in Figure 2 and realized using a different mechanism in the oscillatory interference models.

grated displacement signals from 1D velocity integrators, so the model is named GRIDSmap (Grid Regularity from Integrated Distance through Self-organizing map).

Stripe cells in the model initially project nonspecifically to Layer II cells. Through a process of map self-organization modeled below, the connectivity patterns that correspond to coactivations of stripe cells are reinforced among these projections. Because of the most frequent appearance of coactivations with n = ±1, $m = \pm 2$, the competitive dynamics of self-organizing map learning emphasizes projections from cells with orientations that are ±60° apart over all others, which in turn creates the hexagonal positional representations characteristic of grid cells in Layer II neurons. Figure 3 illustrates these geometrical relationships and Figure 4 provides the circuit diagram for the GRIDSmap model that shows the velocity input processing by stripe cells and the self-organizing map from stripe cells to grid cells.

The model's mathematical equations and simulations that verify the above reasoning are presented in the Methods section and the following section, respectively.

Simulation Settings and Results

Simulations were conducted on three spatial scales. Each spatial scale was treated independently. There is a gradient of spatial scales along the dorso-ventral axis of the entorhinal cortex, and the projections from Layer III to II are local and topographic. For the sake of simplicity, the model assumes that there is no overlap between different spatial scales projecting to a subset of grid cells corresponding to each scale.

Seven simulations were performed to test the model. Each of the seven simulations used four spatial phases of stripe cells for each preferred direction. In each simulation, all stripe cells projected nonspecifically using initial random weights to a self-organizing map layer of putative grid cells. Five putative grid cells were used in all simulations presented here. Simulations differed by the angle of separation between stripe cell preferred directions (and therefore the number of stripe cells), the variation in angle separation, and the spatial scale. The first simulation was set in the ideal conditions where the spatial scale of stripe cells is short ($l = 4$ corresponding to a spatial scale of

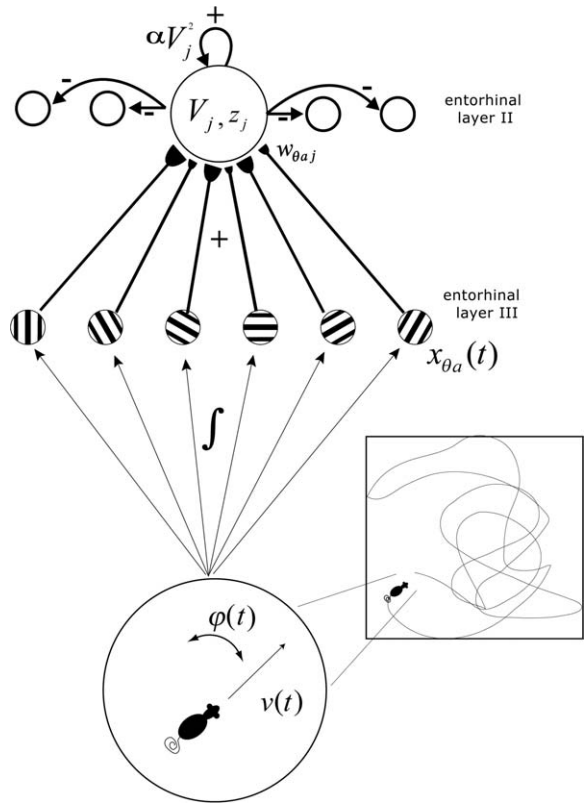

FIGURE 4. Circuit diagram of the GRIDSmap model. As the rat traverses the environment, signals of linear velocity $v(t)$ and angular velocity $\varphi(t)$ are used to generate a one-dimensional periodic path-integrated distance code in the form of stripe cells $x_{\theta a}(t)$ with orientation θ and phase a in Layer III of entorhinal cortex. These cells form the input layer of a two layer self-organizing neural architecture and project nonspecifically to the map layer. The map layer consists of stellate cells (with activations V_j) in Layer II of the entorhinal cortex. Projections have adaptive weights $w_{\theta aj}$ which are governed by a postsynaptically gated competitive learning rule, called the instar learning rule. The stellate cells V_j form a shunting recurrent on-center off-surround winner-take-all network which, in conjunction with this learning rule, enables the Layer II cells to learn the most frequent coactivation patterns in the Layer III stripe cells. A habituative gating mechanism z_j in the Layer II cells enables the map to represent input patterns that it experiences through time without getting stuck in an initially learned bias. See the Methods section for mathematical definitions of all variables.

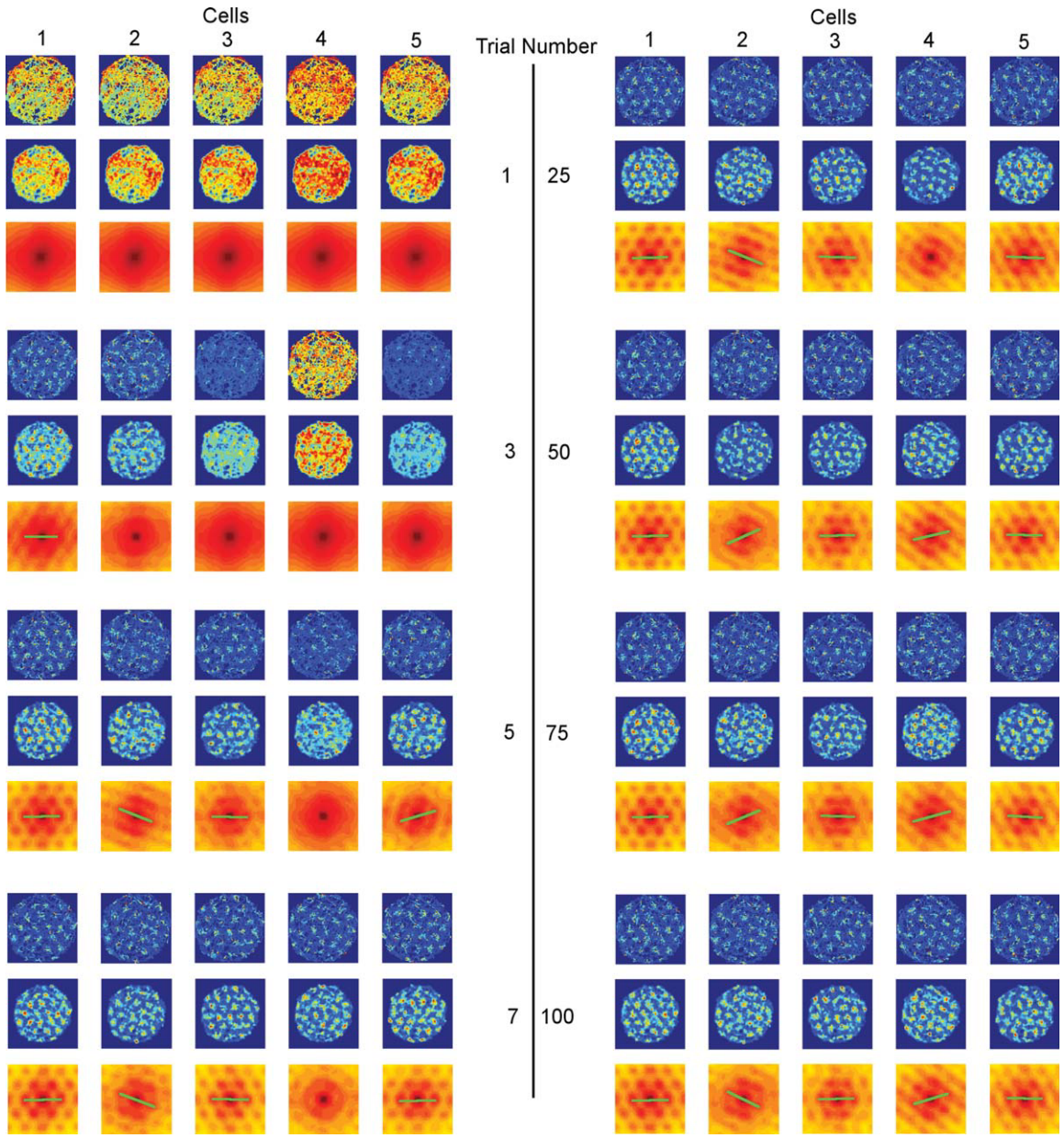

FIGURE 5. Temporal dynamics of grid fields development for a shortest scale. Movement trajectories were derived from experimentally recorded movement information (Sargolini et al., 2006). One hundred successive learning trials were conducted using the same trajectory. Firing fields and autocorrelation maps of all five cells after Trials 1, 3, 5, 7, 25, 50, 75, and 100 are shown with each column in the figure corresponding to a different cell. In each trial, the top row shows the normalized average firing rate map of the cell. The center row shows the normalized rate map smoothed using a Gaussian convolution filter. The bottom row shows the autocorrelation maps of the smoothed rate map. The scale of the stripe cells was controlled by the parameters l and b [in Eqs. (6) and (5), respectively]. These were set to $l = 4$ (spatial scale 20 cm) and $b = 0.5$ in these simulations. The angular separation between stripe cells' preferred directions was fixed at 20°.

20 cm) and the angular separation between stripe cell preferred directions is large (20°). Nine different angles and four spatial phases led to the use of 36 stripe cells in this simulation. The simulation was run for 100 trials. Each trial consisted of the model rat running along a trajectory constructed from experimentally recorded trajectories (Sargolini et al., 2006). To establish the correspondence between the time step in the model (2 μs) and the time step in the experimental trajectory sampling (20 μs), the trajectory data was linearly interpolated to a higher resolution. The results of this simulation are presented in Figures 5 and 6.

Figure 5 presents the cell activities during different trials as well as autocorrelation maps of these activities. The first grid (Cell 1) appears by Trial 3 and remains stable through the rest of the trials in both the positions of the peaks and the orientation. Cell 5 shows a case when the grid is initially formed with

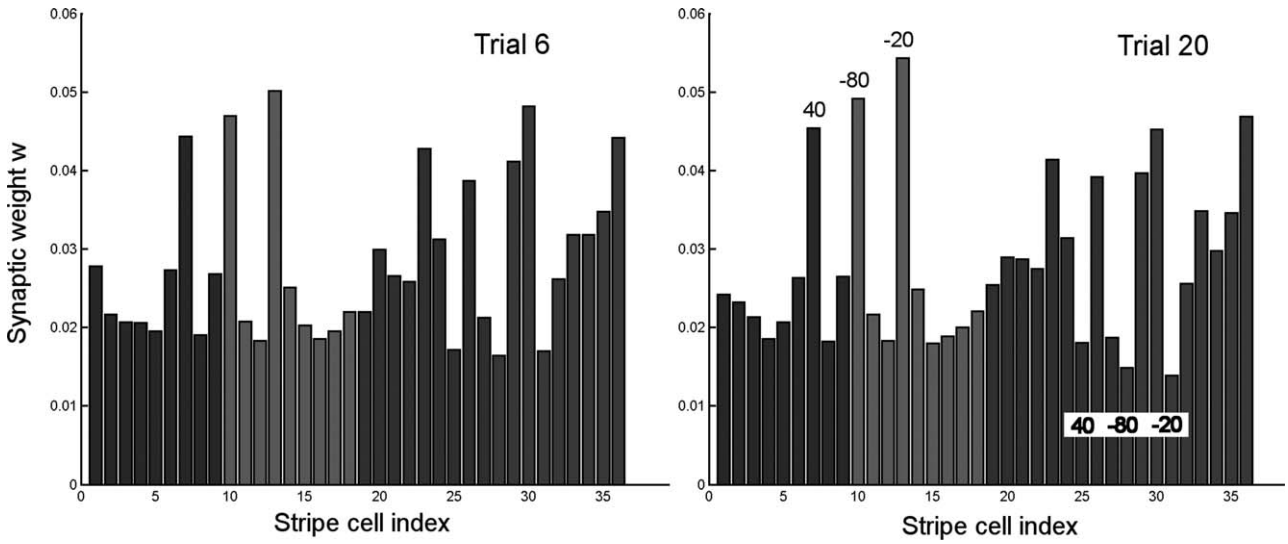

FIGURE 6. Sample synaptic weights developed during simulation. Thirty six synaptic weights of incoming projections to a single grid cell from nine preferred directions and four different phases of stripe cells are shown. Weights are shown after Trial 6 and Trial 20. Four spatial phases are highlighted with four colors of the bars. In each phase, angles go from -80° to 80° with step 20° from left to right. Numbers next to peaks and troughs highlight the respective stripe cell preferred directions.

one orientation (Trial 5), but then realigns with the majority of other grids by Trial 7. Cell 2 shows that if the initial orientation is about 30° away from the majority of other cells, it can get stuck and not realign itself; continuing to be about 30° away from others. Cell 4 is the last to form the grid and also has an orientation that matches Cell 2 rather than Cells 1, 3, and 5. Autocorrelation maps for Cells 2 and 4 appear less stable than for Cells 1, 3, and 5. Note, in addition, that the cells develop with different spatial phases.

Figure 6 shows a set of sample synaptic weights developed during the first 20 trials of this simulation. These weights are taken from Cell 1, which develops the grid by Trial 3. There is no qualitative change in weights between Trials 6 and 20, which shows the stability of the learned grid. Note that weights often form triplets of 60° separation across different spatial phases of stripe cells as shown in Figure 6 with two preferred directions (−20° and −80°) coming from the second spatial phase and one (40°) from the first. This is normal and if the population of grid cells in the model were sufficiently large, one could see all combinations of stripe phases leading to complete coverage of the environment by grid cells. There are also three equally clear troughs for the same preferred directions coming from cells with the opposite spatial phase. Furthermore, a set of less prominent but nevertheless noticeable peaks occur between these troughs with preferred directions of $-60°, \ldots, -40°$, 0°, and 60°. Looking at Figure 5 suggests that these determine the cell orientation, rather than the first set of peaks. Figure 6 illustrates a rare case wherein the tendency to mix different spatial phases and the tendency to have peaks and troughs on the opposite spatial phase are clearly separated. Most of the weight sets are less readable due to mixing angles and rebounds on all phases (results not shown).

The next simulation showed that randomly chosen orientations of stripe cells could nonetheless lead to learning of a hexagonal grid cell firing pattern. In this simulation, the spatial scale was the same ($l = 4$ corresponding to a spatial scale of 20 cm) and nine angles were calculated by taking nine different integers k within $[-4, 4]$ and computing $20°k + \gamma$, where γ is an integer drawn randomly from a uniform distribution on the interval $[-8°, 8°]$. Nine angles with four spatial phases set the number of stripe cells to 36. This and the remaining simulations consisted of 20 trials each. The results of this simulation are presented in Figure 7. Similar to the results in Figure 5, some grids form earlier than others. Cell 2 shows the realignment of the grid closer to the orientation of the majority of other cells. Randomness in the angular separation of stripe cells did not lead to a noticeable deterioration of the resulting grids.

The spatial scale of 20 cm in the simulations shown in Figures 5 and 7 was not observed in rats, where the shortest grid scale is on the order of 30 cm. In the next four simulations, l was increased to 6 (corresponding to a spatial scale of 30 cm). The angular separation between stripe cells' preferred directions was fixed in these simulations at 20°, 15°, 10°, and 7°. As a result, the total number of stripe cells for these simulations was 36, 48, 72, and 104, respectively. Each simulation consisted of 20 trials. The results for these simulations are presented in Figure 8.

Similar to previous simulations, the results show the tendency of orientations to rotate and cluster together. The overall quality of the grids is not as good as for a shorter spatial scale, even for the angular separation of 20°. For 7° of angular separations, the autocorrelation maps appear stripier than for the other 3 cases, although 15° and 10° cases also show stripy patterns for some cells.

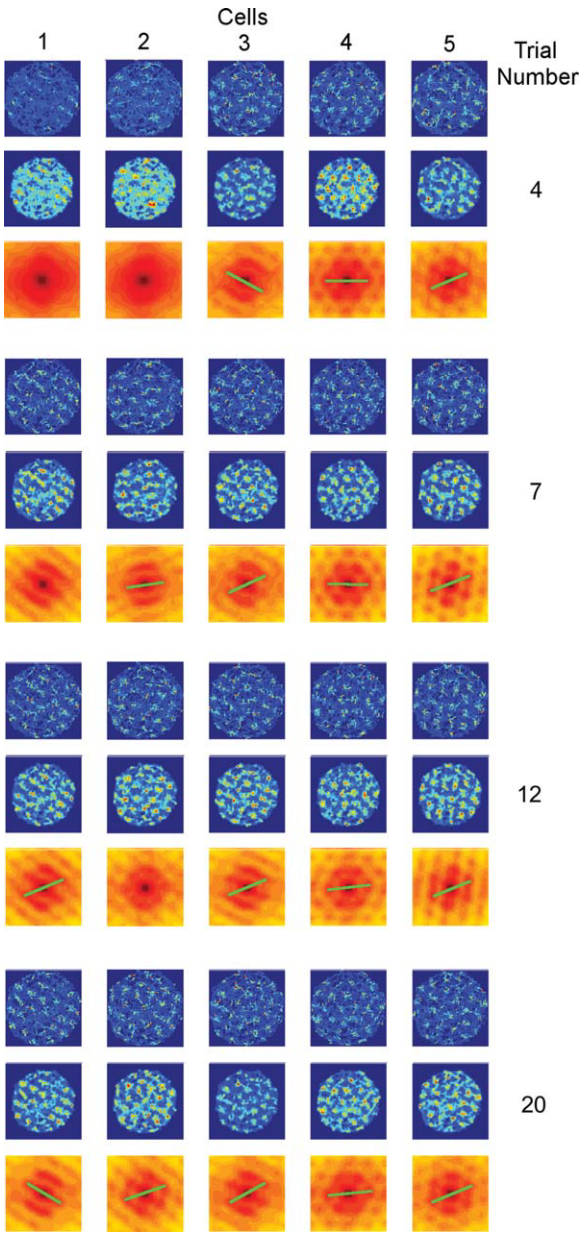

FIGURE 7. Grid fields of a shortest scale with randomized angular separations. The structure of the figure is the same as in Figure 5. The scales of the stripe cells are controlled by the parameters l and b [in Eq. (6) and (5), respectively]. These were set to $l = 4$ (spatial scale 20 cm) and $b = 0.5$ in these simulations. The angular separation between stripe cell preferred directions was randomized as described in the text.

The last simulation used the longest spatial scale of stripe cells ($l = 8$ corresponding to a spatial scale of 40 cm) and the angle separation between stripe cell preferred direction was 20°. The total number of stripe cells was 36. The simulation consisted of 20 trials. The results are presented in Figure 9. Here the grids look fuzzy, but despite that their orientations tend to be aligned close to each other. Testing even larger scales would not be illustrative because the small size of the trajectory will not allow a sufficient number of grid peaks to fall within the covered environment. This will lead to problems during grid development as well as visualization.

DISCUSSION

Multiple Scale Map Learning Rates and Environmental Size

The GRIDSmap model explains how a self-organizing map from stripe cells to grid cells within the entorhinal cortex can lead to the formation of hexagonal grid cell firing fields. This self-organizing map is sensitive to trigonometric properties of spatial navigation which favor cooccurrences of activity representing directions that are separated by 60°. This trigonometric property is model-independent, and may be a fundamental reason for hexagonal firing fields that any grid cell model should be able to incorporate.

A similar self-organizing map from entorhinal grid cells to hippocampal place enables learning of hippocampal place cell fields that can represent a much larger, and behaviorally useful, range of spatial scales than grid cells; namely, place cells whose spatial scale is the least common multiple of the spatial scales of the grid cells that input to them (Gorchetchnikov and Grossberg, 2007). Our current results therefore contribute to a unified theory whereby the wide range of spatial scales observed in the brain that support spatial navigation may result from similar laws of self-organized map learning taking place at successive levels within the entorhino-hippocampal system (Fig. 1). The possible existence of a unified computational entorhinal-hippocampal framework is important to keep in mind when comparing and contrasting the GRIDSmap model with alternative models of grid cells. This fact takes on additional significance when one asks how the self-organized learning in this map hierarchy is dynamically buffered against catastrophic forgetting, as is briefly discussed at the end of this section.

It is also of interest that, because of the sharing of computational mechanisms at multiple stages of the hierarchy, the number of trials of model learning needed to form the grid cells is similar to the number of trials needed to form place fields from grid fields (Gorchetchnikov and Grossberg, 2007). This illustrates how grid cells and the place cells that receive their inputs may, other things being equal, be learned at similar rates as an animal navigates in an environment, thereby enabling place cells that represent large spaces to be learned as the grid cells that support them are learned.

Given that the trajectory was constructed based on experimentally recorded 10 min runs, the simulation length of 20 trials corresponds to a total of 200 min of learning for the grid structure to stabilize. In small scale simulations, grids became mostly stable by the end of the 5th trial, or 50 min of exploration. We are not aware of data which measure precisely how long it takes to form grid cells in newborn animals. In the absence of such data, 50–200 min seems to be a reasonable amount of time, on a behavioral scale, for the formation of

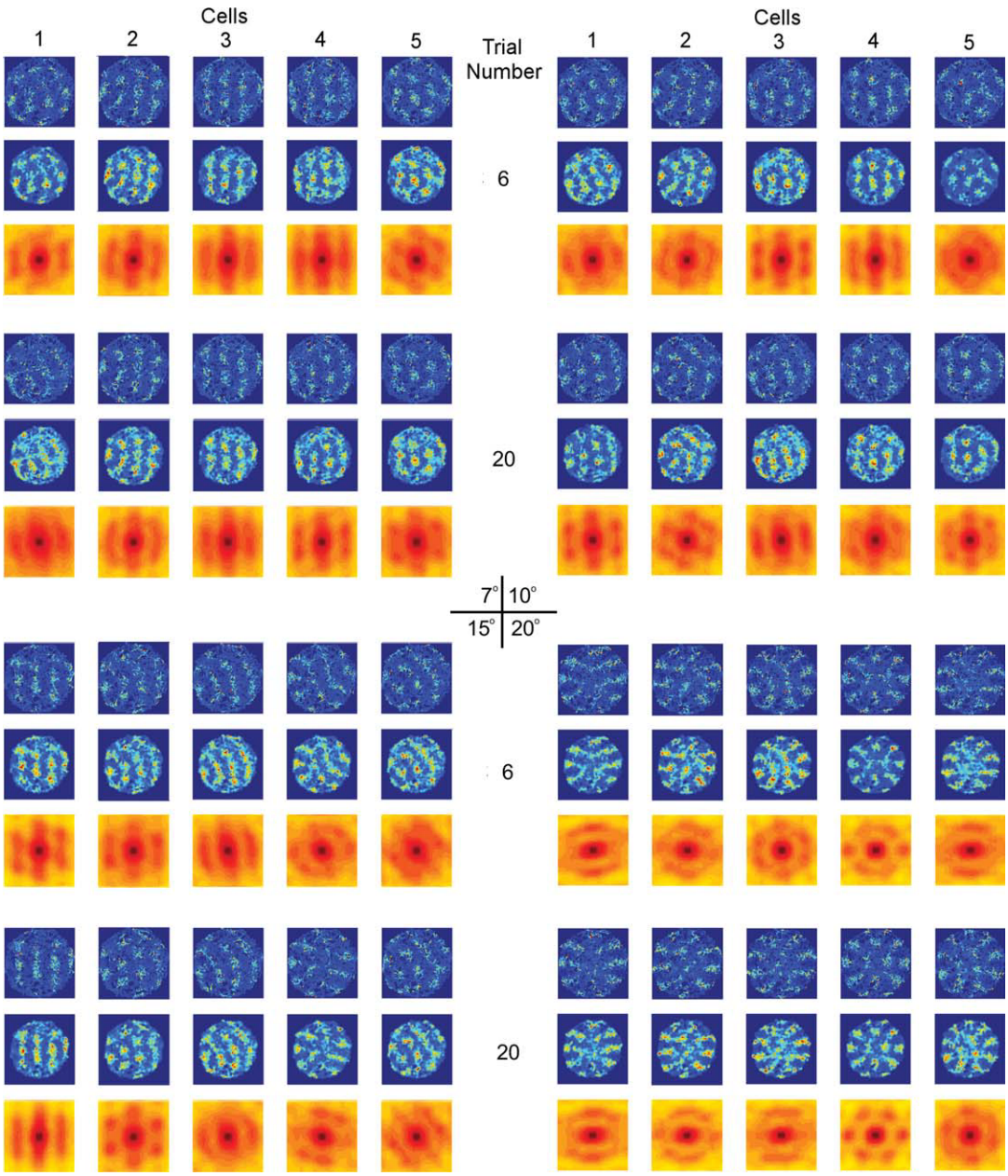

FIGURE 8. Grid fields of an intermediate spatial scale with different angular separations of input. The structure of the figure is the same as in Figure 5. The scales of the stripe cells are controlled by the parameters l and b [in Eq. (6) and (5), respectively]. These were set to $l = 6$ (spatial scale 30 cm) and $b = 1.125$ in these simulations. The angular separation between stripe cell preferred directions was fixed at 7°, 10°, 15°, and 20° and is marked in the middle of the figure.

grid cells. For larger spatial scales, the spatial dimensions of exploration seem to have a stronger influence on the stability of the grid than does the exploration duration. Considering that with a grid scale of 20 cm there are 25 points of coactivation in a 1×1 m^2 environment, one can calculate how much longer it will take for a larger scale to learn equally well. The scale 30 cm will have about nine coactivation points in the same environment, and the scale 40 will have about 6.25 coactivation points. To have equal exposure to coactivation episodes, a rat has to spend 2.7 more time in the environment for a 30-cm scale and 4 times more for 40 cm scale. For the 20 cm scale in the simulations presented here, most grids were stable and well shaped after seven trials. That would mean that the same shape of grids could be achieved by Trial 19 for a 30-cm scale and by Trial 28 for 40-cm scale. As Figure 9 shows, this was not the case. This result leads to the hypothesis that the size of the environment limits the scale of the grids that can be stabilized in this environment. The results of Figures 5 and 9 suggest that stable grids of scale l can be quickly formed in the environments of size $4l$ or larger. Since breeding companies

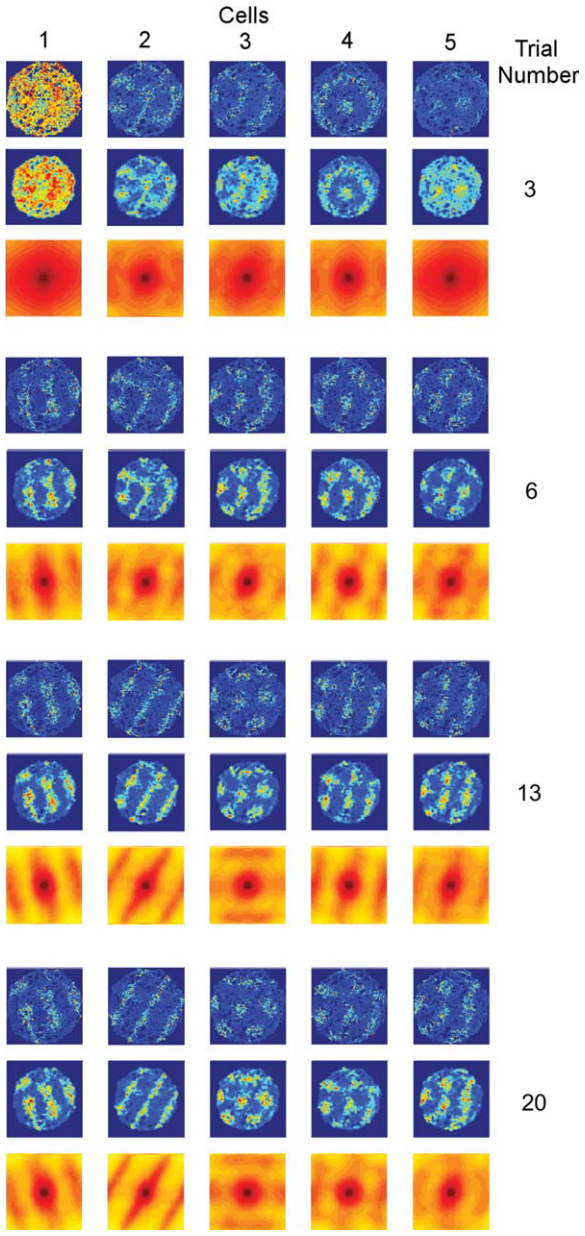

FIGURE 9. Firing fields of a largest spatial scale. The structure of the figure is the same as in Figure 5. The scale of the stripe cells was controlled by the parameters l and b [in Eq. (6) and (5), respectively]. These were set to $l = 8$ (spatial scale 40 cm) and $b = 2$ in these simulations. The angular separation between stripe cell preferred directions was fixed at 20°.

grow rats in small enclosures, this would suggest, other things being equal, that grids of large spatial scales would not be stable until the animal get about 1 h of exposure to a sufficiently large apparatus.

Grid Cell Orientations and Phases

The results presented in Figure 5 illustrate that the GRIDSmap model allows initial development of grid cells with non-identical orientations. This result does not correspond to available experimental data. Our simulation results also show, however, that quite quickly, and more often than not, these orientations align close together. This is the result of competition in the self-organizing map, whereby cells are pushed to have their activities as far from each other as possible, and this leads to a similar orientation/different phase packing. In some cases cell orientations nonetheless get stuck about 30° away from the majority of other cells' orientations.

It is likely that the competition between only five cells is not strong enough to push it out of this local minimum, and that increasing the number of grid cells in GRIDSmap model may lead to more coherent orientations of resulting grids, thereby suggesting the prediction that such competition may be a mechanism that contributes to coherent grid orientations in the brain. The results also suggest that the smaller the angular separation between stripe cells preferred orientations, the tighter the distribution of grid orientations. If during development the brain starts with a lot of different preferred directions of stripe cells, then this trend will lead to better attunement of grids to the same orientations during initial development (cf. the simulations at 7° summarized in Fig. 8). Stripe cells that are not used as inputs to grid cells, because they do not feed the correct orientations, can later gradually die out or retune, which will allow the development of more precise grids (cf. the simulations at 20° summarized in Fig. 8) which inherit the coherent orientations from the first phase.

Note in Figure 5 that the grid cells develop with different spatial phases. This results from competitive selection of favored combinations of inputs from stripe cells with different orientations and spatial phases. The competitive learning dynamics of the self-organizing map hereby generates a network of grid cells with individual hexagonal firing fields at different spatial phases.

By using nonspecific connections with randomly assigned initial connection weights, the GRIDSmap model demonstrates that the observed hexagonal grid structure may be a natural outcome of self-organization and is not a product of either hard-wired design or of specific initial conditions. The possibility of such a self-organization process has been previously discussed by Burgess et al. (2007), but was not explicitly modeled or simulated in previously proposed models of grid cells.

Different Approaches to Velocity Integration

The mechanism of velocity integration proposed by GRIDSmap model differs from the mechanisms proposed by previous models. Blair et al. (2008) used 1D ring attractors defined by oscillators whose displacement information is encoded in the phases of the oscillations, which is decoded into positional information by oscillatory interference. In GRIDSmap, the position of the activity bump along stripe cells directly represents the position of the animal along the preferred direction. The model's self-organizing map detects and enhances the most frequent co-occurrences of these positional activations. Continuous attractor models accomplish the integration on the level of

grid cells and in 2D (Fuhs and Touretzky, 2006; Burak and Fiete, 2009). The interference model uses a velocity-based input to alter the frequency of oscillations to accomplish the integration (Burgess, 2008). The persistent firing version of the interference model uses the firing properties of entorhinal cells to integrate velocity (Hasselmo, 2008), although these properties were also shown to integrate velocity outside of the interference model paradigm (Hasselmo and Brandon, 2008). Stripe cells within the GRIDSmap model integrate velocity in 1D and these signals are then input to the grid cells, just as in the interference models. In contrast with interference models, the current model uses network properties of the ring attractors to perform the integration, similar to continuous attractor models, and this integration is complete within the stripe cell 1D attractor and does not require any further postprocessing on the level of grid cells, thus making integration and grid formation independent of each other.

Integration of velocity signals has been observed in other parts of the brain and is often modeled using 1D attractors. For example, computational models have shown how head direction cells in the lateral mammilary nuclei could integrate angular head velocity signals to compute allocentric head direction using a 1D ring attractor (Skaggs et al., 1995; Redish et al., 1996; Boucheny et al., 2005; Song and Wang, 2005). A similar 1D ring attractor mechanism within the entorhinal cortex could be responsible for integrating linear velocity signals that are modulated by head direction signals to compute directional displacement.

Other Grid Cell Models

Two main types of models that have been proposed in the past to address the problem of how the grid cell firing structure could form. The continuous attractor model (Fuhs and Touretzky, 2006; McNaughton et al., 2006; Burak and Fiete, 2009) of grid cell proposes that grid cell firing may be due to network-level dynamics resulting from recurrent connectivity within the population of grid cells. The grid pattern is maintained using symmetrically weighted connections between the cells, while a set of asymmetrically weighted connections allow the activity pattern to shift based on velocity signals. The model maintains the periodic grid structure and performs path integration with respect to the animal's movement. The network connections are finely tuned and the asymmetric weights distributed in a tailored manner across cells (Fuhs and Touretzky, 2006). This level of precision in connection weights is required for the dynamics of this model to function effectively and might be difficult to justify in a biological context without additional simulations showing how this weight structure can be formed in a natural way. A more recent version of this model uses more realistic connections, but also requires specific tuning of these connections to achieve correct path integration under aperiodic boundary conditions (Burak and Fiete, 2009). While periodic boundary conditions achieve better performance for their model, Burak and Fiete (2009) consider the underlying connectivity as too complex to be realistic. Replacing a 2D attractor with a set of 1D stripe cell attractors as proposed here allows the to use of periodic boundary conditions in a setting where they are more realistic than for 2D attractors, and inherits all the advantages of attractor models with periodic boundary conditions.

Interference models propose that the grid pattern arises due to interference between a base oscillation frequency and multiple oscillations that have frequencies which are sensitive to velocity and head direction (Burgess et al., 2007; Hasselmo et al., 2007; Burgess, 2008). There is evidence for subthreshold oscillations in dMEC Layer II stellate cells (Alonso and Klink, 1993; Klink and Alonso, 1997b). Furthermore, the frequencies of these oscillations correlate with the positions of cells along a dorso-ventral axis of the entorhinal cortex, and thus with the spatial scale of the grid (Giocomo et al., 2007).

To generate the hexagonal pattern, another requirement of the interference model is the selective combination of the head direction modulation, which has to come from head direction cells with preferred directions that are 60° apart from each other. The interference model so far assumes that these specific head directions are selected as inputs through some self-organization process (Burgess et al., 2007). Other directions lead to dramatically different grid cell firing fields that have not been observed (Hasselmo et al., 2007). Furthermore, while algorithmic level designs of this model have successfully shown a grid structure in multiple settings, a biophysically based model of this theory has not been published. As these algorithmic implementations are sensitive to noise (Hasselmo, 2008), the conversion of the model to a biological context might not function robustly. Implementation of self-organized learning similar to GRIDSmap in the framework of the interference model might help to overcome at least some of these concerns.

A basic problem addressed by all current models of grid cell formation is how to translate velocity-dependent path integration inputs into positional information. The interference model does so altering the phase of oscillators that have a baseline oscillatory frequency. Blair et al. (2008) implement this using 1D ring attractors. The GRIDSmap model also uses 1D ring attractors that integrate linear velocity into a moving activity bump that directly codes linear displacement. GRIDSmap ring attractors share many design features with 1D ring attractors that have been used to model head direction cells (Taube et al., 1990; Skaggs et al., 1995; Redish et al., 1996; Song and Wang, 2005), which use an activity bump to code angular displacement. Thus, GRIDSmap proposes a computationally parsimonious scheme for linear and angular velocity integration as a substrate for grid cell learning. Various 2D continuous attractor models directly shift an attractor bump representing position using velocity-based inputs.

Experimental Support for Velocity-Based Input

Any path integration model, including the interference model, the continuous attractor models, and the GRIDSmap model, depends critically on the velocity-dependent input signal to the entorhinal cortex. The interference model puts addi-

tional constraints on this signal since it is used to alter the subthreshold oscillation frequency of the entorhinal cells in a precise fashion. Sharp et al. (2006) reported about 10% of cells in lateral habenula as having firing rate correlates with the running speed, but these cells project to modulatory systems including cholinergic nuclei and are more likely to affect the base theta frequency than the intrinsic oscillation frequency in the entorhinal cells. O'Keefe et al. (1998) reported rare encounters of a velocity-dependent signal in the hippocampal formation (they did not specify the recording site), and attributed these recordings to the inputs from caudate nucleus. Another path to provide a linear velocity to the entorhinal cortex goes through the fastigial nucleus and the lateral nuclei of the thalamus.

Experimental Support for Stripe Cells

Some evidence for the existence of cells with stripe-like firing fields is found in experimental results reporting the properties of conjunctive cells in Layers III, V, and VI of the dorsal segment of medial entorhinal cortex (dMEC; Sargolini et al., 2006). Conjunctive cells have both directional and spatial specificity. Some of these cells have a stripe-like cell firing field reflected in their autocorrelograms, although it does not necessarily mean that their firing profile is also arranged in parallel stripes. Band cells formed by oscillatory interference with similar activity were proposed in some versions of the interference model of Burgess et al. [(2007), Fig. 2a; (Burgess, 2008), Fig. 2f]. Further studies are needed to verify the existence of either band or stripe cells. It is possible that a stripe or band structure will appear most clearly if one measures them relative to theta phase timings of the corresponding cell spikes [(Burgess, 2008), Fig. 2e; (Hasselmo, 2008), Fig. 2b]. Cells in Layer III of the entorhinal cortex show theta phase modulation in their firing. They are more restricted to a specific phase in the beginning and the end of firing and have a broader phase in the middle of firing (Hafting et al., 2008). Thus if one considers only the firing on the phase opposite of the starting phase, the firing field will look like a stripe in the middle of actual firing field.

For simplicity, the GRIDSmap model does not investigate spike timings and uses a rate-based model similar to the thresholding used by Burgess (2008) to convert between his Figure 2e showing phase-based stripe cells and Figure 2f showing firing field-based stripe cells.

Similarities and Differences Between GRIDSmap and Other Models

The GRIDSmap model shares some key concepts with both interference and attractor models. A major tenet of both GRIDSmap and interference models is the existence of velocity-dependent stripe or band cells, which in both models perform the role of 1D linear velocity integration, albeit using different mechanisms. Also, according to both models, the spatial scale of the grid cells derives from the spatial scale (frequency in the interference model) of the stripe (band) cells. Therefore, it is predicted that these stripe cells also exhibit a gradient of spatial scales as is observed in the grid cells. Furthermore, the grid patterns in both models will be altered if inputs from multiple stripe cells with identical preferred directions and spatial phases would be provided to the grid cell. In response to such inputs, the map cells will follow the stripe firing pattern of the inputs rather than creating a grid. In the simulations presented here, only one stripe cell per preferred direction and phase combination was used. Local competitive interactions between stripe cells can lead to an outcome where, for a given set of projections, there is only one stripe cell per preferred direction and phase combination. Future simulations are necessary to define the specifics of such a network.

The GRIDSmap model includes two levels of attractor dynamics. On the grid cell level, attractor dynamics are a key component of self-organizing maps (Grossberg, 1976a,b, 1978). Furthermore, just as integration of angular velocity in head direction cells can be modeled by a moving bump ring attractor model (Taube et al., 1990; Skaggs et al., 1995; Redish et al., 1996; Song and Wang, 2005), the GRIDSmap model suggests that linear velocity integration in stripe cells may also use a moving bump ring attractor circuit. Burak and Fiete (2009) showed that a 2D continuous attractor model with periodic boundaries has several advantages over a network with aperiodic boundaries. GRIDSmap does not combine velocity integration and grid formation in one stage like 2D attractor models. The 1D ring attractors proposed in GRIDSmap allow the advantages of periodic boundaries without requiring the complex toroidal connectivity of 2D attractor. Furthermore, combining three 1D displacements on a 2D plane introduces the redundancy that can serve as an additional error correction mechanism for path integration.

Blair et al. (2008) also proposed 1D ring attractors to provide inputs to grid cells. In this version of the interference model, these rings are tonically active, velocity-controlled oscillators that code position by oscillatory phases. These phases are then decoded into hexagonal patterns of grid cell firing by oscillatory interference. In GRIDSmap, the 1D ring attractors are phasically activated velocity integrators that code position in an activity bump on each 1D ring attractor. Here a hexagonal pattern of grid cell firing arises from the most frequent cooccurrences of these 1D positional activations, with less frequent or weaker cooccurrences suppressed by an interaction of competitive, habituative, and associative dynamics. Future experimental work is needed to determine if 1D velocity integration is done through an interference mechanism that leads to band cells, or through an attractor mechanism that leads to stripe cells. In either case, the self-organized learning proposed by the GRIDSmap model will function robustly.

Model Extensions: Top-Down Feedback for Self-Stabilizing Map Memory and Oscillations

Top-down feedback pathways exist within the entorhinal-hippocampal system (e.g., Fig. 1). On the basis of previous analyses of how such feedback pathways work (Grossberg, 1976a,b, 1980, 1999; Carpenter and Grossberg, 1987, 1991), one can

conclude that the feedback pathways from hippocampus to entorhinal cortex may help to explain how place cell selectivity can be learned within seconds to minutes, yet can remain stable for months (Thompson and Best, 1990; Wilson and McNaughton, 1993; Muller, 1996; Frank et al., 2004). This combination of fast learning and stable memory is often called the stability–plasticity dilemma (Grossberg, 1980, 1999). Self-organizing maps are themselves insufficient to solve the stability-plasticity dilemma in a dense input environment that experiences changing statistics, as occurs regularly during real-world navigation. However, self-organizing maps augmented by learned top-down expectations that focus attention upon expected combinations of features can do so. Such a self-organizing map model, augmented by feedback from hippocampus to entorhinal cortex (Grossberg, 2009), has already helped to explain the pattern of beta frequency oscillations that is observed during place cell learning in a novel environment (Berke et al., 2008). Although a systematic study of these feedback pathways is outside the scope of the current model, the existence of such pathways may help to clarify a number of important properties of grid and place cell learning, stability, and remapping that go beyond the predictive range of the GRIDSmap model, including how multiple grid cells across the entorhinal cortex quickly learn to share the same orientation preference.

Beta oscillations coexist with a number of other types of oscillatory dynamics in the entorhinal-hippocampal system. As noted above, the interference model includes explanations of how theta frequency may be modulated at different spatial scales. Preliminary simulations have shown that the habituative mechanisms of the GRIDSmap model can generate oscillations if the model input is provided as a constant current injection, thereby emulating an in vitro recording environment where such oscillations have been observed experimentally (Giocomo et al., 2007). Indeed, habituative dynamics in competitive recurrent on-center off-surround networks, such as those which occur in self-organizing maps, have long been known to be capable of complex oscillatory dynamics (e.g., Carpenter and Grossberg, 1983, 1984a,b, 1985). These observations point the way toward the development of a unified hierarchy of self-organizing maps, augmented by top-down attentive feedback, and interacting with mechanisms of visually-based navigation and cognitive planning, to explain a wide variety of data about spatial navigation.

METHODS

Network Description

Stripe cells

To simplify model computations, as in Blair et al. (2008), the simulations presented here do not explicitly simulate 1D ring attractors but rather approximate their output by the following mechanism. Let $x_{\theta a}$ be a stripe cell oriented along the allocentric direction θ, with spatial phase a, and period l. The cell $x_{\theta a}$ is defined to have maximal activity at periodic positions $d_\theta = nl + a$ for all integer values of n within its firing field. In other words, cell $x_{\theta a}$ will fire maximally whenever (d_θ modulo l) $= a$, where the modulo operator computes the remainder when d_θ is divided by l. For simplicity, the experimental data distances and spatial scales in the simulations were calculated in units of 5 cm, so that $l = 4$ means a spatial scale of 20 cm. To determine when a strip cell fires as an animal navigates, its velocity and distance traveled need to be computed relative to stripe cell receptive field properties.

If at time t the animal is moving along a direction $\varphi(t)$ with speed $v(t)$, then the velocity v_θ along direction θ is:

$$v_\theta(t) = \cos(\theta - \varphi(t))v(t). \tag{3}$$

The distance d_θ, traversed along direction θ is calculated by integrating the velocity:

$$d_\theta(t) = \int_0^t v_\theta(\tau)d\tau, \tag{4}$$

and then resetting the distance modulo the period l. This periodically reset distance is:

$$s_{\theta a}(t) = (d_\theta(t) - a) \text{ modulo l}. \tag{5}$$

The spatial scale l is not incorporated explicitly into the notation $s_{\theta a}$ for simplicity. Thus, if the stripe cell has a Gaussian-like firing profile, then its activity can be modeled as:

$$x_{\theta a}(t) = e^{\frac{-\left(s_{\theta a}(t) - \frac{l}{2}\right)^2}{b}}. \tag{6}$$

A Gaussian profile is chosen because of it natural occurrence in many cell firings, including 1D ring attractors. Blair et al. (2008) used a cosine profile in modeling their ring attractor signals, which was more suitable for their oscillatory model.

The distance variables $d_\theta(t)$ were all initialized to 0.5, which corresponds to 2.5 cm. This value was initially selected so that the starting activity of all stripe cells in the first simulation with $l = 4$ (spatial scale 20 cm) was minimal (0.5 is exactly in-between two spatial phases). Starting with $d_\theta(t)$ initially set to zero would cause maximal initial activity in the stripe cell with phase a equal 0. Subsequent simulations of different scales showed that, as long as $d_\theta(t)$ is shifted from zero by some small amount, the model is able to perform the task, so there was no need to set it at exactly half-length of a spatial phase.

For simulations of multiple different scales, the scale of the stripe cell was increased by increasing the ratio of l_0 to another scale l_1 by an a factor (1.5 or 2 in two different simulations) and simultaneously increasing the ratio of the width b_0 of the Gaussian in (5) to b_1 so that $\frac{l_0}{l_1} = \sqrt{\frac{b_0}{b_1}}$ holds true.

Map cells

The activation V_j of the entorhinal II map cell j is defined by an on-center off-surround network whose cells obey membrane, or shunting, dynamics:

TABLE 1.

Parameter Values Common Across All Simulation Trials are Shown

A	B	D	η	β	p_{kj} $(k \neq j)$	p_{kj} $(k = j)$	α	λ	Time step (ms)
3	1	1.5	0.4	0.2	1.5	0	17.5	0.0025	0.02

The same values were used for simulations across the different scales. Integration was done using Euler's method and the respective time step is given.

$$\frac{dV_j}{dt} = -AV_j + (B - V_j)\left(\sum_{\theta a} w_{\theta aj} x_{\theta a} + \alpha[V_j]^{+2}\right) z_j - (D + V_j)\sum_k p_{kj}[V_k]^{+2}. \quad (7)$$

In (7), A is the decay rate corresponding to the leak conductance, B and $-D$ are excitatory and inhibitory saturation levels corresponding to respective reversal potentials, $w_{\theta aj}$ is the synaptic weight from stripe cell $x_{\theta a}$, $[V_j]^{+2}$ is the thresholded on-center self-excitatory feedback, where $[V_j]^{+} = \max(V_j, O)$, with gain coefficient α which allows the cell to maintain persistent activity, z_j is a habituative transmitter gate, p_{kj} is the inhibitory connection strength which multiplies the inhibitory signal $[V_k]^{+2}$ from cell k in the off-surround to cell j. The recurrent self-excitation could also be realized by a nonspecific cation after depolarization (ADP) current shown to exist in Layer II stellate cells (Klink and Alonso, 1997a; Egorov et al., 2002) and modeled in applications to grid cells by Hasselmo (2008). Index θ goes through orientations on the interval [-90° 90°) in steps corresponding to the specific simulation setup. Note that 0° is used in all simulations and the other directions are counted from it. Index a goes through spatial phases, 0 to l in steps of $l/4$. Index k goes through 5 entorhinal II map cells. The recurrent on-center off-surround network with a nonlinear signal function such as V^2 enables the most highly activated cell to win the competition and suppress less activated cells, thereby triggering learning at the adaptive weights which drive the winning cell (Grossberg, 1976a,b, 1978; Kohonen, 1984).

Adaptive weights

The adaptive weights $w_{\theta aj}$ of axonal connections from stripe cells to entorhinal II map cells are governed by a competitive instar learning rule (Grossberg, 1976a,b, 1980; Carpenter and Grossberg, 1987).

$$\frac{dw_{\theta aj}}{dt} = \lambda[V_j]^{+2}\left(x_{\theta a}\left(2 - \sum_{pq} w_{pqj}\right) - w_{\theta aj}\sum_{p\neq,q\neq a} x_{pq}\right), \quad (8)$$

where λ is the learning rate. In (8), learning is gated on and off by the postsynaptic cell output signal $[V_j]^{+2}$ When a cell j wins the competition, it can hereby trigger learning. All the adaptive weights $w_{\theta aj}$ whose axons abut cell j compete for a conserved amount of total synaptic weight, scaled to 2 in (8). Increasing one weight decreases the other weights via the competitive inhibitory term $w_{\theta aj}\sum_{p\neq,q\neq a} x_{pq}$ Note that this is not a passive decay. It is active competition for a conserved maximal synaptic weight. If there is no activity in any of the other stripe cells, there will not be any synaptic depression at this synapse. Moreover, the rate of learning depends on the current state of the weights. If the cell already has well developed weights, then the cell has low plasticity unless new inputs can successfully drive a redistribution of already committed adaptive weights.

The adaptive weights $w_{\theta aj}$ were initialized to random values drawn from a uniform distribution in the interval [0.005, 0.01]. The interval for drawing was set based on the number of the stripe cells in the 7° simulation. The upper bound was selected so that the maximum of the total initial sum of weights is less than 2. The lower bound was set to a half of the upper bound. With these initial values, the learning law ensures that the total sum of the weights remains less than 2 for all time.

Habituative gates

A habituative transmitter gate z_j in Eq. (7) prevents cells which win the competition early on from persistently winning and thereby preventing other cells from participating in map learning (Grossberg, 1980; Olson and Grossberg, 1998; Grossberg and Seitz, 2003). With transmitter habituation, all map cells can undergo similar amount of learning. Also when an animal remains stationary, habituative gating reduces the activity of the active grid cell. This reduces learning during stationary periods so that persistent activity will not drive the synaptic potentiation or depression to unreasonable levels. In this regard, the gates does not shut down completely, so that the grid cell will continue firing when the animal is stationary, but at a lower rate. This prediction of the model can be tested experimentally. The habituative transmitter gate is defined by:

$$\frac{dz_j}{dt} = \eta\left((1 - z_j) - \beta z_j\left(\sum_{\theta a} w_{\theta aj} x_{\theta a} + \alpha[V_j]^{+2}\right)^2\right), \quad (9)$$

where η is the rate of activation/deactivation of the gate, term $(1-z_j)$ defines the transmitter recovery rate to a target Level 1, β scales the input- and positive-feedback-dependent rate of habituation $\left(\sum_{\theta a} w_{\theta aj} x_{\theta a} + \alpha[V_j]^{+2}\right)^2$, which is the signal that z_j gates in Eq. (7).

Spatial scales

The spatial scale of the stripe cells was determined by setting the values of l and b in Eqs. (5) and (6) and the four spatial

phases were determined by setting the values of a [Eq. (5)] to $nl/4$ where $n = \{0, 1, 2, 3\}$, and 4 is the number of spatial phases.

Parameter values are summarized in Table 1. Integration was performed using Euler's method.

Postprocessing

The rate map provides a measure of the average model activity in small regions of space. It is used to illuminate the model's grid structure as the model animal navigates around the simulated enclosure. The rate map is created by binning the 2D environment into 6,400 squares (80 horizontal by 80 vertical, each bin corresponding to a 1.125×1.125 cm^2 in the experimental environment used by Sargolini et al. (2006). If R_{ij} are the different bins, with i and j ranging from 1 to 80, and $\tau(t)$ is the position of the rat at time t on the trajectory, then the average model activity X_{ij} in the bin R_{ij} is,

$$X_{ij} = \frac{\sum\limits_{t \in T_{ij}} V_k(t)}{\left|T_{ij}\right|}, \tag{10}$$

where $T_{ij} = \{t{:}\tau(t) \in R_{ij}\}$. See Figures 3 and 4, left column. The rate map is smoothed using a 2D Gaussian convolution:

$$Y_{ij} = \sum_g \sum_h X_{ij}.G(g-i, h-j) \tag{11}$$

where

$$G(g,h) = e^{\frac{-(g^2+h^2)}{2\sqrt{9}^2}}, \tag{12}$$

and g and h range from -8 to +8. See Figures 3 and 4, middle column. The autocorrelation between the fields with spatial lags of x and y was estimated as

$$r(x,y) = \frac{\sum\limits_n Y_{ij} Y_{i-x,j-y}}{\sum\limits_n Y_{ij}^2 \sum\limits_n Y_{i-xj-y}^2}, \tag{13}$$

where the summation is over all n bins of $\{R_{ij}\}$ where rates for both Y_{ij} and $Y_{i-x,j-y}$ are present.

Acknowledgment

The authors thank anonymous reviewers for valuable comments on the manuscript.

REFERENCES

Alonso A, Klink R. 1993. Differential electroresponsiveness of stellate and pyramidal-like cells of medial entorhinal cortex layer II. J Neurophysiol 70:128–143.

Berke JD, Hetrick V, Breck J, Green RW. 2008. Transient 23- to 30-Hz oscillations in mouse hippocampus during exploration of novel environments. Hippocampus 18:519–529.

Blair HT, Gupta K, Zhang K. 2008. Conversion of a phase- to a rate-coded position signal by a three-stage model of theta cells, grid cells, and place cells. Hippocampus 18:1239–1255.

Boucheny C, Brunel N, Arleo A. 2005. A continuous attractor network model without recurrent excitation: Maintenance and integration in the head direction cell system. J Comput Neurosci 18:205–227.

Burak Y, Fiete IR. 2009. Accurate path integration in continuous attractor network model of grid cells. PLoS Comput Biol 5:e1000291.

Burgess N. 2008. Grid cells and theta as oscillatory interference. Theory and predictions. Hippocampus, 18:1157–1174.

Burgess N, Barry C, Jeffery KJ, O'Keefe J. 2005. A grid and place cell model of path integration utilizing phase precession versus theta. Computational Cognitive Neuroscience Meeting, Washington, DC.

Burgess N, Barry C, O'Keefe J. 2007. An oscillatory interference model of grid cell firing. Hippocampus 17:801–812.

Carpenter GA, Grossberg S. 1983. A neural theory of circadian rhythms: The gated pacemaker. Biol Cybernet 48:35–59.

Carpenter GA, Grossberg S. 1984a. A neural theory of circadian rhythms: Aschoff's rule in diurnal and nocturnal mammals. Am J Physiol 24:R1067–R1082.

Carpenter GA, Grossberg S. 1984b. A neural theory of circadian rhythms: Split rhythms, after-effects, and motivational interations. J Theor Biol 113:163–223.

Carpenter GA, Grossberg S. 1987. A massively parallel architecture for a self-organizing neural pattern recognition machine. Comput Vis Graph Image Process 37:54–115.

Carpenter GA, Grossberg S. 1991. Pattern Recognition by Self-Organizing Neural Networks. Cambridge, MA: MIT Press.

Egorov AV, Hamam BN, Fransén E, Hasselmo ME, Alonso AA. 2002. Graded persistent activity in entorhinal cortex neurons. Nature 420:173–178.

Frank LM, Stanley GB, Brown EN. 2004. Hippocampal plasticity across multiple days of exposure to novel environments. J Neurosci 24:7681–7689.

Fuhs MC, Touretzky DS. 2006. A spin glass model of path integration in rat medial entorhinal cortex. J Neurosci 26:4266–4276.

Giocomo L, Zilli E, Fransen E, Hasselmo M. 2007. Temporal frequency of subthreshold oscillations scales with entorhinal grid cell field spacing. Science 315:1719–1722.

Gorchetchnikov A, Grossberg S. 2007. Space, time, and learning in the hippocampus: How fine spatial and temporal scales are expanded into population codes for behavioral control. Neural Networks 20:182–193.

Grossberg S. 1976a. Adaptive pattern classification and universal recoding, I: Parallel development and coding of neural feature detectors. Biol Cybernet 23:121–134.

Grossberg S. 1976b. Adaptive pattern classification and universal recoding, II: Feedback, expectation, olfaction, and illusions. Biol Cybernet 23:187–202.

Grossberg S. 1978. A theory of human memory: Self-organization and performance of sensory-motor codes, maps, and plans. In: Rosen R, Snell F, editors. Progress in Theoretical Biology, Vol. 5. New York: Academic Press. pp 233–374. (Reprinted in 1982. Grossberg S. Studies of Mind and Brain. Kluwer/Reidel).

Grossberg S. 1980. How does the brain build a cognitive code? Psychol Rev 87:1–51.

Grossberg S. 1999. The link between brain learning, attention, and consciousness. Consciousness Cogn 8:1–44.

Grossberg S. 2009. Beta oscillations and hippocampal place cell learning during exploration of novel environments. Hippocampus 19:881–885.

Grossberg S, Seitz A. 2003. Laminar development of receptive fields, maps, and columns in visual cortex: The coordinating role of the subplate. Cereb Cortex 13:852–863.

Hafting T, Fyhn M, Molden S, Moser MB, Moser E. 2005. Microstructure of the spatial map in the entorhinal cortex. Nature 436:801–806.

Hafting T, Fyhn M, Bonnevie T, Moser MB., Moser EI. 2008. Hippocampus-independent phase precession in entorhinal grid cells. Nature 453:1248–1252.

Hasselmo M. 2008. Grid cell mechanisms and function: Contributions of entorhinal persistent spiking and phase resetting. Hippocampus 18:1213–1229.

Hasselmo ME, Brandon MP. 2008. Linking cellular mechanisms to behavior: Entorhinal persistent spiking and membrane potential oscillations may underlie path integration, grid cell firing, and episodic memory. Neural Plasticity 2008:658323.

Hasselmo M, Giocomo L, Zilli E. 2007. Grid cell firing may arise from interference of theta frequency membrane potential oscillations in single neurons. Hippocampus 17:1252–1271.

Klink R, Alonso A. 1997a. Muscarinic modulation of the oscillatory and repetitive firing properties of entorhinal cortex layer II neurons. J Neurophysiol 77:1813–1828.

Klink R, Alonso A. 1997b. Ionic mechanisms of muscarinic depolarization in entorhinal cortex layer II neurons. J Neurophysiol 77:1829–1843.

Kohonen T. 1984. Selforganization and Associative Memory. Berlin: Springer-Verlag.

McNaughton BL, Battaglia FP, Jensen O, Moser EI, Moser MB. 2006. Path integration and the neural basis of the "cognitive map." Nat Rev Neurosci 7:663–678.

Mhatre H, Gorchetchnikov A, Grossberg S. 2009a. Hexagonal structure of grid cells formed by fast self-organized learning within the entorhinal cortex. Proc Annu Conf Soc Neurosci 679.6.

Mhatre H, Gorchetchnikov A, Grossberg S. 2009b. A neural model of grid cell hexagonal map formation by self-organized learning. Proc Comput Cogn Neurosci Conf (Abstract 39).

Muller RA. 1996. A quarter of a century of place cells. Neuron 17:813–822.

O'Keefe J, Burgess N, Donnet JG, Jeffery KJ, Maguire EA. 1998. Place cells, navigational accuracy, and the human hippocampus. Philos Trans R Soc Lond B 353:1333–1340.

Olson S, Grossberg S. 1998. A neural network model for the development of simple and complex cell receptive fields within cortical maps of orientation and ocular dominance. Neural Networks 11:189–208.

Redish AD, Elga AN, Touretzky DS. 1996. A coupled attractor model of the rodent head direction system. Network Comput Neural Syst 7:671–685.

Rolls ET, Stringer SM, Elliot T. 2006. Entorhinal cortex grid cells can map to hippocampal place cells by competitive learning. Network Comput Neural Syst 447:447–465.

Sargolini F, Fyhn M, Hafting T, McNaughton B, Witter M, Moser MB, Moser EI. 2006. Conjunctive representation of position, direction, and velocity in entorhinal cortex. Science 321:58–762.

Skaggs W, Knierim JJ, Kudrimoti HS, McNaughton BL. 1995. A model of the neural basis of the rat's sense of direction. Adv Neural Inform Process Syst 7:173–182.

Sharp PE, Turner-Williams S, Tuttle S. 2006. Movement related correlates of single cell activity in the interpeduncular nucleus and habenula of the rat during a pellet chasing task. Behav Brain Res 166:55–70.

Solstad T, Moser EI, Einevoll GT. 2006. From grid cells to place cells: A mathematical model. Hippocampus 16:1026–1031.

Song P, Wang XJ. 2005. Angular path integration by moving "hill of activity": A spiking neuron model without recurrent excitation of the head-direction system. J Neurosci 25:1002–1014.

Taube JS, Muller RU, Ranck Jr JB. 1990. Head-direction cells recorded from the post subiculum in freely moving rats. J Neurosci 10:420–435.

Thompson LT, Best PJ. 1990. Long-term stability of the place-field activity of single units recorded from the dorsal hippocampus of freely behaving rats. Brain Res 509:299–308.

Wilson MA, McNaughton BL. 1993. Dynamics of the hippocampal ensemble code for space. Science 261:1055–1058.